The Journal of Experimental Biology 216, 1458-1469

doi:10.1242/jeb.079855

RESEARCH ARTICLE

# Active downward propulsion by oyster larvae in turbulence

Heidi L. Fuchs[1,*], Elias J. Hunter[1], Erika L. Schmitt[2] and Regina A. Guazzo[1]

[1]Institute of Marine and Coastal Sciences, Rutgers University, New Brunswick, NJ 08901, USA and [2]St Mary's College of Maryland, St Mary's City, MD 20686, USA

*Author for correspondence (hfuchs@marine.rutgers.edu)

## SUMMARY

**Oyster larvae (*Crassostrea virginica*) could enhance their settlement success by moving toward the seafloor in the strong turbulence associated with coastal habitats. We characterized the behavior of individual oyster larvae in grid-generated turbulence by measuring larval velocities and flow velocities simultaneously using infrared particle image velocimetry. We estimated larval behavioral velocities and propulsive forces as functions of the kinetic energy dissipation rate ε, strain rate γ, vorticity ξ and acceleration α. In calm water most larvae had near-zero vertical velocities despite propelling themselves upward (swimming). In stronger turbulence all larvae used more propulsive force, but relative to the larval axis, larvae propelled themselves downward (diving) instead of upward more frequently and more forcefully. Vertical velocity magnitudes of both swimmers and divers increased with turbulence, but the swimming velocity leveled off as larvae were rotated away from their stable, velum-up orientation in strong turbulence. Diving speeds rose steadily with turbulence intensity to several times the terminal fall velocity in still water. Rapid dives may require a switch from ciliary swimming to another propulsive mode such as flapping the velum, which would become energetically efficient at the intermediate Reynolds numbers attained by larvae in strong turbulence. We expected larvae to respond to spatial or temporal velocity gradients, but although the diving frequency changed abruptly at a threshold acceleration, the variation in propulsive force and behavioral velocity was best explained by the dissipation rate. Downward propulsion could enhance oyster larval settlement by raising the probability of larval contact with oyster reef patches.**

Key words: acceleration, *Crassostrea virginica*, dissipation rate, force balance, larval behavior, velocity gradients.

Received 5 September 2012; Accepted 17 December 2012

## INTRODUCTION

Many mollusc veligers change their behavior in response to turbulence, and variations in these responses provide clues to whether or how adult habitat structure shapes larval behavior. Veligers pull in the velum and sink when disturbed (Barile et al., 1994; Young, 1995), but reactions to turbulence vary among species from enclosed habitats *versus* exposed coastlines. For example, mud snails (*Ilyanassa obsoleta*) and blue mussels (*Mytilus edulis*) inhabit estuaries or inlets with energetic tidal currents, and larvae of these species swim up in calm water but sink in turbulence above a threshold value of the turbulent kinetic energy dissipation rate ε (Fuchs et al., 2004; Fuchs and DiBacco, 2011). These behaviors could raise the probability of being retained near and settling in turbulent coastal inlets (Fuchs et al., 2007; Fuchs and DiBacco, 2011). Snail larvae (*Crepidula* spp. and *Anachis* spp.) from subtidal beaches behave differently, sinking in calm water and swimming up in strong turbulence (Fuchs et al., 2010). These genus-specific responses to turbulence suggest that larval behaviors may be adapted for settlement into distinct adult habitat types. Here, we studied larval responses to turbulence in a reef-building bivalve, the eastern oyster *Crassostrea virginica*. Oyster larvae undergo rapid downward accelerations, termed 'dive bombing' (Finelli and Wethey, 2003), but the trigger for diving is unknown. We hypothesize that oyster larvae dive in response to turbulence as a way of concentrating near the bottom despite vigorous mixing over the rough substrates created by oyster reefs.

It is generally assumed that veliger larvae descend in turbulence by passive gravitational sinking. Passive descents are a reasonable assumption because veligers are negatively buoyant and sink by arresting the ciliary beat or retracting the velum when disturbed or presented with chemical cues in still water (e.g. Fretter, 1967; Cragg, 1980; Hadfield and Koehl, 2004). Water motion makes it more difficult to observe the cilia and velum, however, and active descents cannot be ruled out without estimates of propulsive force under realistic flow conditions. The downward accelerations observed in oyster larvae (Finelli and Wethey, 2003) could indicate an abrupt behavioral change from upward swimming to passive sinking, an abrupt reduction in upward propulsive force, or a change in the direction of propulsion. Propulsive force can be estimated from measured velocities of larvae and the flow around them. Such measurements are difficult, and previous studies on larvae in turbulence described larval behavior only in terms of behavioral velocities (Fuchs et al., 2004; Fuchs et al., 2010; Fuchs and DiBacco, 2011).

Here, we describe both larval behavioral velocity and propulsive forces in turbulence, and this added complexity calls for a definition of terms to distinguish among modes of behavior. We use 'ascent' or 'descent' to refer to a positive or negative vertical velocity due to larval propulsion. These behavioral velocities are exclusive of fluid motions and are distinct from the net larval velocity due to the combined motions of larvae and fluid. We define 'swimming' and 'diving' as propulsive forces directed upward and downward,

respectively, relative to the larval axis. By this definition, swimmers can ascend or descend, depending on the magnitude of propulsive force relative to the combined opposing forces of drag and gravity. We use 'sinking' to refer only to those larvae descending passively without propulsion.

Previous studies described larval responses to turbulence only as a population- and time-averaged function of the dissipation rate. The dissipation rate is a good descriptor of larval-scale turbulence because it defines the Kolmogorov length, time and velocity scales: $\eta_k=(\nu^3/\varepsilon)^{0.25}$, $\tau_k=(\nu/\varepsilon)^{0.5}$ and $\upsilon_k=(\nu\varepsilon)^{0.25}$, respectively, where $\nu$ is kinematic viscosity (see List of symbols). These scales represent the smallest eddies with which larvae may interact. Larvae respond rapidly to instantaneous cues (e.g. Hadfield and Koehl, 2004; Koehl and Hadfield, 2010), so although population-average behaviors are useful for modeling settlement processes (Fuchs et al., 2007), average behaviors may be unrepresentative of larval reactions to instantaneous turbulence. Moreover, we suspect that larvae cannot detect the dissipation rate itself but rather sense and respond to more specific flow characteristics such as the strain rate $\gamma$ (deformational shear), vorticity $\xi$ (rotational shear) or acceleration $\alpha$ (e.g. Kiørboe et al., 1999). These velocity gradients probably elicit behavioral changes when the magnitudes of $\gamma$, $\xi$ or $\alpha$ exceed the larval detection limits or response thresholds. If larvae react to instantaneous velocity gradients, then time-resolved observations are needed to characterize responses to turbulence.

Larvae potentially sense turbulence with the velar cilia, used for swimming and feeding, or with statocysts, used to detect gravity (Chia et al., 1981). Some veligers have mechanosensory cilia that stop beating or draw inwards when touched (Murakami and Takahashi, 1975; Mackie et al., 1976; Dickinson, 2002). Deformation of the cilia could enable larvae to sense strain rates, or the whole ciliated velum could act as an antenna to detect spatial variability in the shear. Statocysts could sense changes in orientation (vorticity-induced rotation) or changes in velocity (acceleration). Veligers have an asymmetric density distribution and normally swim with the velum facing up, but they can rotate away from this passively stable orientation when the viscous torque due to vorticity or shear across the body exceeds the gravitational torque (Kessler, 1986; Jonsson et al., 1991). Vorticity and acceleration would likely be sensed only with the statocyst, whereas strain rate may be detectable both by the cilia as deformation and by the statocysts as axial rotation. Pinpointing the sensing mechanism will require an understanding of which velocity gradients elicit changes in behavior.

We investigated the behavioral responses of oyster larvae to dissipation rates and velocity gradients. Larval velocities and water velocities were measured simultaneously using infrared particle-image velocimetry (IR PIV) (e.g. Catton et al., 2007; Sutherland et al., 2011), and larval propulsive forces were estimated using an expanded equation of particle motion. These detailed measurements enabled us to characterize the velocities and propulsive forces of individual larvae as a response to instantaneous flow characteristics. This combined study of behavioral velocities and propulsive forces adds a new dimension to our insights into how larvae respond to turbulence.

## MATERIALS AND METHODS

Behaviors of eyed oyster larvae (*C. virginica* Gmelin 1791) were characterized in both still water and turbulence. We measured water velocities and larval velocities simultaneously using near-IR PIV. This method requires seeding the flow with particles, illuminating a plane with a laser light sheet, and taking pairs of images separated by a small time step. The image pairs are used to calculate water velocities in the plane based on the motions of seeding particles within small interrogation areas (Adrian, 1991). Seeding particles could alter larval behavior, so in summer 2010 we characterized behavior of larvae in still water with different particle types. In April 2011 we carried out turbulence experiments in a grid-stirred tank.

Larvae were shipped overnight from Horn Point Laboratory and used within 48 h. Before use, larvae were kept in 10 l cultures at 20°C and a salinity of 9.5 $S_P$ with Shellfish Diet (Reed Mariculture, Campbell, CA, USA) mixed algae for food. All experiments were done at room temperature (21–22°C) and a salinity of 9.5 $S_P$.

### Still-water experiments

For still-water experiments, larvae were added to 8 liter aquaria containing no particles (control) or one of three different particle types: mixed algae (3–18 μm, ~1.07 g cm$^{-3}$, Shellfish Diet), hollow glass spheres (12 μm, ~1.1 g cm$^{-3}$, Sphericel, Potters Industries LLC, Valley Forge, PA, USA) or nylon particles (20 μm, ~1.03 g cm$^{-3}$, PSP, Dantec Dynamics Inc., Holtsville, NY, USA). Larval and particle concentrations were 0.3–0.7 larvae ml$^{-1}$ and $5.0\times10^4$ cells ml$^{-1}$, respectively. The particle concentrations were comparable to typical feeding concentrations for larval cultures and the concentrations of seeding particles required for PIV. No-particle controls were replicated nine times, and particle treatments were replicated six times. For each treatment we used an infared LED spotlight to illuminate the aquarium and video-recorded larval motions for 12–15 min at a frame rate of 3 Hz using a digital video camera (KPF-120, Hitachi Ltd, Tokyo, Japan) and capture software (XCAP, EPIX Inc., Buffalo Grove, IL, USA). We later reconstructed the larval trajectories ($N$=18–3498 per replicate) using a custom particle-tracking algorithm in Matlab (e.g. Fuchs et al., 2004) to estimate larval velocities.

Larvae were subsampled after each replicate for measurement of shell length and terminal sinking velocity. Shell length ($N$=30–35 per replicate) was measured digitally using a stereomicroscope and software (M205C and Leica Application Suite, Leica, Wetzlar, Germany). Fall velocity ($N$=47–124 per replicate) was measured from digital video of ethanol-killed larvae sinking through a 2 liter settling column at room temperature and a salinity of 9.5 $S_P$.

### Turbulence experiments

Turbulence experiments were done in a 170 liter tank (46 cm wide × 46 cm deep × 80 cm high) with turbulence generated by vertical oscillation of two horizontal stirring grids. The grids had a mesh size of 6.35 cm, a grid separation distance of 40.6 cm and an oscillation amplitude of 12.7 cm. Six different stirring frequencies were used, ranging from $f$=0.02 to 1.61 Hz. Unlike tanks with a single stirring grid (e.g. Hopfinger and Toly, 1976; Brumley and Jirka, 1987), tanks with two stirring grids produce turbulence that is homogeneous and nearly isotropic in a large region centered between the two grids (Srdic et al., 1996; Shy et al., 1997).

Measurements were made with an IR PIV system that included a pulsed diode laser (NanoPower 7 W, 808 nm) with a ~2 mm beam width and a 4 megapixel camera (FlowSense, Dantec Dynamics) with a 55 mm lens (Leica). We used ~18 μm concentrated algae (*Thalassiosira weissflogii*, Reed Mariculture) as seeding particles because artificial particles induced behavioral changes in still-water experiments. A foam lid was used to dampen secondary flows. The PIV image plane (5 cm high × 10 cm wide) was centered at $z$=20.3 cm from each grid and 13 cm from each of the nearest walls, an offset of 10 cm from the center. The horizontal offset was necessary because the IR laser light attenuated with distance from the source and was too weak in the center of the tank. The images

were far enough from the walls that larval motions were free of wall effects (Vogel, 1994).

Two replicates were done using larval concentrations of 0.5 and 0.3 larvae ml$^{-1}$, respectively. For the first replicate we used six, randomly ordered turbulence levels. A 10 min warm-up period at the beginning of each treatment ensured that the turbulence was stationary. For the second replicate we used a different treatment order but were only able to complete three turbulence treatments because of an equipment malfunction. At each turbulence level we collected 10 min of PIV data at 10 Hz (i.e. 10 image pairs per second), observing hundreds to thousands of individual larvae per treatment. All data were combined in our analysis.

### Image processing

The PIV images of larvae in turbulence represent a two-phase flow, with larvae and fluid moving in different directions, so we separated the images of larvae and tracer particles (e.g. Kiger and Pan, 2000) to quantify larval and fluid motions. Before calculating the fluid velocity vectors we equalized the image backgrounds, removed noise and masked out the larvae to obtain good estimates of background fluid flow and to limit error in the calculation of individual larval velocities. The image intensity varied spatially because of IR light attenuation, so we were unable to use standard procedures of subtracting the mean background intensity of each individual image and removing pixel-scale noise with a median filter (Khalitov and Longmire, 2002; Cheng et al., 2010). Instead, we equalized the background by calculating the mean image intensity over each 10 min sampling interval and subtracting the mean intensity from each image, repeating for frame 1 and frame 2 images. The particle image intensity also varied spatially, so we used wavelet analysis (e.g. Torrence and Compo, 1998; Weng et al., 2001) to remove the noise based on its spatial scale while ignoring spatial variability in particle image intensity. To reduce noise in the images we decomposed each image using Coiflet wavelets (Mohideen et al., 2008), removed wavelet coefficients below a scale threshold and reconstructed the image from the remaining signal. The resulting images had a relatively constant background intensity, were free of small-scale noise, and retained the scale and intensity of the particle images.

We also had to remove larvae from the images, because larval velocities often exceeded or opposed the underlying flow velocities. Larval particle images sometimes became saturated and had a bright, reflective halo, so we first applied a 2-dimensional, high-pass, fast Fourier transform filter that reduced the halo effect. After filtering, we removed the residual background by squaring the image intensity and setting to zero any pixel intensities below a threshold. Lastly, we binarized the images, identified and labeled each particle, and classified particles with area >10 pixels as larvae. Larval particle images were removed, leaving images of only seeding particles.

### Fluid velocities and turbulence

The paired images of seeding particles were processed using adaptive correlation algorithms in Dynamic Studio (Dantec) to calculate velocity vectors $u$ and $w$ in the $x$ and $z$ directions, respectively. We used interrogation areas of 64×64 pixels at the two lowest settings and 32×32 pixels at higher settings with a 50% overlap to give vector resolutions of $\Delta x$=0.16 cm and $\Delta x$=0.08 cm, respectively. These resolutions gave the best balance between improving the quality of vector calculations and limiting the difference between the vector spacing $\Delta x$ and Kolmogorov length scale $\eta_k$.

We used measured fluid velocity gradients to calculate the 2-dimensional Eulerian acceleration $\alpha$, strain rate $\gamma$, horizontal component of vorticity $\xi$ and dissipation rate $\varepsilon$ in the neighborhood of individual larvae. The acceleration, strain rate and vorticity are given by:

$$\alpha = \left[ \left( \frac{\partial u}{\partial t} \right)^2 + \left( \frac{\partial w}{\partial t} \right)^2 \right]^{0.5} , \quad (1)$$

$$\gamma = \frac{1}{2} \left( \frac{\partial u}{\partial z} + \frac{\partial w}{\partial x} \right) , \quad (2)$$

$$\xi = \frac{\partial w}{\partial x} - \frac{\partial u}{\partial z} . \quad (3)$$

We calculated the dissipation rate directly from measured velocity gradients as:

$$\varepsilon(x,z) = \nu \left[ 8 \overline{\left( \frac{\partial u}{\partial x} \right)^2} - \overline{\left( \frac{\partial w}{\partial z} \right)^2} + 2 \overline{\left( \frac{\partial u}{\partial z} \right)^2} + 2 \overline{\left( \frac{\partial w}{\partial x} \right)^2} \right] \quad (4)$$

(George and Hussein, 1991). This form is simplified from the 3-dimensional definition of dissipation rate using the continuity equation and the assumption that the flow is symmetric about the $z$-axis, such that gradients along the $x$-axis have similar magnitudes to those along the $y$-axis (Taylor, 1935; George and Hussein, 1991). Fluid velocities and turbulence characteristics were later interpolated to the positions of individual larvae.

### Larval behavioral velocities

Larval velocities were calculated by reconstructing larval trajectories from the original images. Larvae were much larger than the algal seeding particles and were easily classified based on their equivalent spherical diameter, solidity and eccentricity. We analyzed only larvae with area >20 pixels that could be tracked unequivocally between paired frames and from image pair to image pair. Paired frames 1 and 2 were treated as frames of two separate image sequences. We reconstructed the larval trajectories in each sequence by particle tracking in Matlab and then matched larvae in the two sequences to get paired trajectories offset by $\delta t$, the time between paired frames. Larvae with trajectories in only one sequence or with trajectories of unequal lengths in the two sequences were excluded from the analysis. We analyzed the paired trajectories of 6355 larvae, including 40,268 instantaneous observations. Trajectory durations ranged from 0.89±1.21 s (mean ± 1 s.d.) at the lowest turbulence level to 0.29±0.16 s at the highest turbulence level.

To limit velocity errors, we estimated larval velocities from the sequence trajectories rather than from movements between paired frames. Particle displacements have uncertainty due to errors in the calculation of particle centroid positions (±0.1–0.25 pixels) (Wernet and Pline, 1993; Adrian, 1997), but these uncertainties can be offset by using a longer time step to increase the dynamic velocity range (Adrian, 1997). The larvae had an average image diameter of 10.8 pixels, or about 549 μm, and the time between image pairs was $\Delta t$=0.1 s, giving a velocity-error standard deviation of $1.6\times10^{-3}$ cm s$^{-1}$ [eqns 2,3 in Adrian (Adrian, 1997)].

Although larval velocities were calculated from sequence trajectories, water velocities and flow statistics were calculated by PIV from each image pair. To characterize the instantaneous flow corresponding to each larva's velocity, we interpolated the water velocities, $u$ and $w$, and the turbulence characteristics, $\alpha$, $\gamma$, $\xi$ and $\varepsilon$, to the larval positions at each time step. We used an unweighted

linear interpolation because it gave results nearly identical to those from a more accurate spline interpolation and required less computation time. The interpolated water velocities and turbulence characteristics were then averaged for each larval trajectory segment.

We estimated larval behavioral velocities as $u_b=u_o-u$ and $w_b=w_o-w$, where $u_o$ and $w_o$ are the observed horizontal and vertical velocities from larval trajectories and $u$ and $w$ are instantaneous fluid velocities interpolated to larval positions. Behavioral vertical velocities $w_b$ are a vector sum of the vertical velocity the larva generates by propulsion and the gravitational sinking velocity. These estimates require the assumption that larval velocities and fluid velocities are additive (e.g. Reeks, 1977). Because larvae are denser than seawater, however, they will have some additional 'slip' velocity when the water accelerates (e.g. Maxey and Riley, 1983; Kiørboe and Visser, 1999). Here, we were unable to separate the behavioral velocity from the slip velocity because flow was unsteady. We estimated the maximum slip velocities for individual larvae assuming steady-state acceleration [eqns 12–15 in Kiørboe and Visser (Kiørboe and Visser, 1999)] and found that the average slip velocity was <1% of the estimated behavioral velocity. Given that the slip velocity was small compared with behavioral velocity, the omission of slip velocity contributes negligible uncertainty to our analysis.

We used paired trajectories to calculate the larval Lagrangian accelerations. The net larval acceleration is $\mathrm{d}\vec{V}_o/\mathrm{d}t=(\vec{V}_{o2}-\vec{V}_{o1})/\delta t$, where $\vec{V}_o=\vec{V}_b+\vec{V}_f$ is the observed translational velocity, $\vec{V}_b$ is the behavioral component of the larval translational velocity, $\vec{V}_f$ is the fluid velocity at the larva's location, an over-arrow denotes a vector, and the subscripts 1 and 2 indicate the sequence number. Here $\vec{V}_o$, $\vec{V}_b$ and $\vec{V}_f$ are 2-dimensional projections of 3-dimensional motion. Sequence 2 was used only for calculating larval accelerations. All other calculations were based on sequence 1 trajectories, and sequence subscripts are omitted hereafter.

The larval vertical velocity appeared to change above a threshold level of turbulence, so we modeled the vertical behavioral velocity using a sigmoidal function (Fuchs and DiBacco, 2011):

$$w_b = b_0 + \frac{b_1}{1+b_2\left(\mathbf{x}/\mathbf{x}^*\right)^{-b_3}} , \tag{5}$$

where $b_0$ is the maximum ascent velocity and $b_0+b_1$ is the maximum descent speed. The fraction $1/[1+b_2(\mathbf{x}/\mathbf{x}^*)^{-b3}]$ varies from 0 to 1, $\mathbf{x}$ can represent $\alpha$, $\gamma$, $\xi$ or $\varepsilon$, and $\mathbf{x}^*$ is a reference value. We used $\alpha^*=1\,\mathrm{cm\,s^{-2}}$, $\gamma^*=1\,\mathrm{s^{-1}}$, $\xi^*=1\,\mathrm{s^{-1}}$ and $\varepsilon^*=1\,\mathrm{cm^2\,s^{-3}}$. This model has upper and lower bounds that account for physical limits on larval swimming, sinking or diving speeds. Before fitting the model we averaged the observed larval vertical velocities over small bins of each turbulence characteristic, where each bin contained 300 instantaneous observations. We fitted Eqn 5 to the bin-averaged larval velocities *versus* each turbulence characteristic using non-linear regression in Matlab. Finally we set $w_b=0$ and solved Eqn 5 for $\mathbf{x}$ to estimate the critical values $\mathbf{x}_{cr}$ of each turbulence characteristic. A critical value represents the threshold of $\mathbf{x}$ at which the average behavioral vertical velocity switches from positive to negative.

### Force balance and terminal velocity

In turbulence, larvae descended at speeds exceeding their terminal fall velocity in still water, suggesting that larvae propelled themselves downward, so we estimated the propulsive force of individual larvae using a force balance equation. Larval movements can be described by the governing equation of motion for small, spherical particles (e.g. Maxey and Riley, 1983; Mei et al., 1991) with additional terms for inertia and propulsion:

$$m\frac{\mathrm{d}\vec{V}_o}{\mathrm{d}t} = \vec{F}_A + \vec{F}_P + \vec{F}_W + \vec{F}_D + \vec{F}_B + \vec{F}_F + \vec{F}_V , \tag{6}$$

where $m$ is the larval mass, $\vec{F}_A$ is the added mass or acceleration reaction force, $\vec{F}_P$ is the pressure gradient force, $\vec{F}_W$ is the net gravitational force due to a larva's weight, $\vec{F}_D$ is the viscous Stokes drag force, $\vec{F}_B$ is the Basset or Boussinesq force, $\vec{F}_F$ is the form drag force and $\vec{F}_V$ is the velar propulsive force. The added mass term is the force required for a larva to displace the water that it moves through:

$$\vec{F}_A = -\frac{2}{3}\pi r^3 \rho_f \frac{\partial \vec{V}_b}{\partial t} , \tag{7}$$

where $r$ is the larval radius and $\rho_f=1.005\,\mathrm{g\,cm^{-3}}$ is the fluid density. The force due to pressure gradients in the fluid is:

$$\vec{F}_P = \frac{4}{3}\pi r^3 \rho_f \frac{\partial \vec{V}_f}{\partial t} . \tag{8}$$

The weight force due to gravity and buoyancy is the excess mass multiplied by gravitational acceleration:

$$\vec{F}_W = \frac{4}{3}\pi r^3 \left(\rho_p - \rho_f\right)\vec{g} , \tag{9}$$

where $\vec{g}=980\,\mathrm{cm\,s^{-1}}$ is the downward acceleration due to gravity and $\rho_p$ is the larval density. The viscous drag force is:

$$\vec{F}_D = -6\pi\mu r\vec{V}_b \tag{10}$$

(e.g. Rubey, 1933) where $\mu$ is dynamic viscosity. The Basset force accounts for historical effects of unsteady drag on the boundary layer around a particle (e.g. Mei et al., 1991) and is given by:

$$\vec{F}_B = -6r^2\left(\pi\rho_f\mu\right)^{0.5}\int_0^t \frac{\mathrm{d}\vec{V}_b}{\mathrm{d}t'}\frac{1}{\left(t-t'\right)^{0.5}}\mathrm{d}t' . \tag{11}$$

The form drag force $\vec{F}_F$ accounts for pressure drag and is given by:

$$\vec{F}_F = -\pi\rho_f r^2 \vec{V}_b^2 \tag{12}$$

(Rubey, 1933). Eqn 12 is similar to the Oseen correction but has a different coefficient and performs better than the Oseen correction at higher particle Reynolds numbers (e.g. Guo, 2011). Particle Reynolds number is $Re_p=\mathrm{d}||\vec{V}_b||/\nu$, where $d$ is the larval shell length and double vertical brackets indicate a vector magnitude.

Force terms in Eqn 6 can be neglected if they are much smaller than the viscous drag force (e.g. Armenio and Fiorotto, 2001). The Basset force and viscous drag were of similar order at $Re_p<1$, the viscous drag dominated at $1\leq Re_p<12$, and the form drag dominated at $Re_p\geq 12$. The forces due to added mass and pressure gradients were small compared with the drag forces, so we omitted them, leaving a final force balance of:

$$m\frac{\mathrm{d}\vec{V}_o}{\mathrm{d}t} = \vec{F}_W + \vec{F}_D + \vec{F}_B + \vec{F}_F + \vec{F}_V \tag{13}$$

(Fig. 1A). We measured or estimated all terms in Eqns 9–13 except $\vec{F}_V$, enabling us to solve Eqn 13 for $\vec{F}_V$ to estimate the magnitude and direction of larval propulsive force.

In still water, the velum faces upward because the centers of buoyancy and gravity are separated by a distance $L$, with the shell acting as a keel, but shear across the body can rotate the larvae away from the normal velum-up orientation (Jonsson et al., 1991).

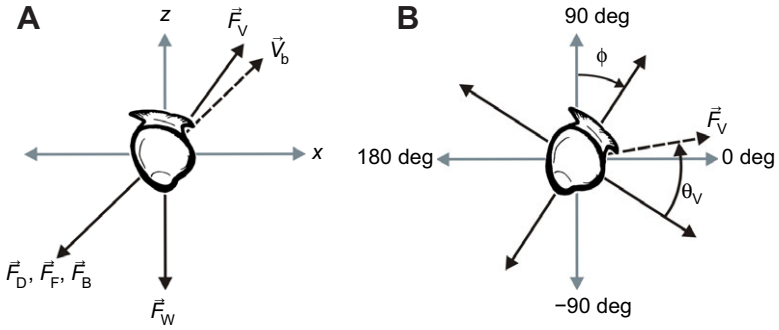


Fig. 1. Diagram of (A) the forces acting on a larva and (B) the angles of larval rotation and propulsion. The forces acting on a larva are the weight force $\vec{F}_W$, the viscous drag force $\vec{F}_D$, the form drag force $\vec{F}_F$, the Basset history force $\vec{F}_B$ and the velar propulsive force $\vec{F}_V$. Added mass $\vec{F}_A$ and pressure gradient forces $\vec{F}_P$ were excluded from the analysis and are omitted. The behavioral component of larval translational velocity is $\vec{V}_b$, the angle of rotation by vorticity is $\phi$ and the direction of propulsion relative to the larval axis is $\theta_V$.

We estimated the larval angle $\phi$ of rotation relative to the passively stable, velum-up orientation (Fig. 1B) as:

$$\sin\phi = \frac{3\mu\xi}{L\rho_p g} \quad (14)$$

(e.g. Kessler, 1986). This equation gives the axial rotation angle when the viscous torque and gravitational torque are at equilibrium. If the vorticity is large enough that the right-hand side of Eqn 14 is >1, there is no equilibrium and the larvae tumble over and over. Although the flow was unsteady, we assumed that larval re-orientation was rapid enough that Eqn 14 represented a good first-order approximation of the rotation angle. We used $\phi$ to convert the Cartesian direction of propulsion to the direction of propulsion relative to the larval axis $\theta_V$ (Fig. 1B). The value of $L$ was unknown but is typically a small percentage of the radius (Kessler, 1986; Jonsson et al., 1991). We assumed $L \approx 3$ μm, or about 1% of the larval length. To characterize the sensitivity of $\theta_V$ to $L$, we also estimated the direction of propulsive forces for $L$ ranging from 1.5 to 6 μm (0.5–2% of the shell length).

For passively sinking larvae, the terminal fall velocity $w_s$ can be estimated using Eqn 13 by setting the accelerations and propulsive force to zero and solving $\vec{F}_W = -\vec{F}_D - \vec{F}_F$ for larval velocity. The resulting equation is Rubey's modification of Stokes law for spherical particles:

$$w_s = -\frac{\sqrt{\frac{4}{3}\|\vec{g}\| r^3 \rho_f (\rho_p - \rho_f) + 9\mu^2} - 3\mu}{r\rho_f} \quad (15)$$

(Rubey, 1933). Terminal velocity estimates from Rubey's equation are lower than those from Stokes law, which overestimates larval fall velocity (e.g. Schwalb and Ackerman, 2011). Rubey's equation accurately predicts the settling velocities of sand grains of up to a few hundred micrometers in diameter (Rubey, 1933; Gibbs et al., 1971) and should work well for larvae. To estimate larval density, we solved Eqn 15 for $\rho_p$ using the shell lengths and terminal velocities measured for dead larvae from the still-water experiments. For the turbulence experiments we measured only the shell lengths ($N$=34, $d$=291±13.0 μm), so we used the measured $d$ and the previously estimated $\rho_p$ in Eqn 15 to estimate the terminal velocity of larvae observed in turbulence.

## RESULTS

### Larval behavior in still water

Still-water experiments confirmed that the presence of artificial particles altered larval behavior (Table 1). Larvae in controls and algal treatments had similar average density, terminal velocity, swimming velocity, direction of motion, sinking frequency and propulsive force. Larval density estimates ($\rho_p$=1.15±0.02 g cm$^{-3}$) were in the range reported previously for bivalve veligers ($\rho_p$=1.1–1.22 g cm$^{-3}$) (Jonsson et al., 1991; Finelli and Wethey, 2003; Schwalb and Ackerman, 2011). Larval propulsion was directed upward in 98% of the larvae, yet the average swimming velocities were near zero and slightly negative, indicating a mix of ascending and descending swimmers. Larvae in the glass and nylon particle treatments had more positive swimming velocities and used more propulsive force than those in controls or algal treatments. Most notably, far fewer larvae were observed in the artificial particle treatments than in controls or algae treatments. The number of tracks, normalized by the number of larvae, video recording time, and image area, was an order of magnitude lower in the glass and nylon particle treatments than in the control and algae treatments. This result supports our qualitative observation that when exposed to glass or nylon particles, many larvae sank immediately to the bottom and remained there, suggesting an adverse reaction to artificial particles.

### Turbulence

Turbulence treatments spanned a wide range of turbulence conditions, with fluid Reynolds numbers ranging from $Re$=36 to

Table 1. Results of still-water experiments: larvae-only controls and larvae plus algae, hollow glass spheres and nylon particles

| Particles | $d$ (μm) | $\rho_p$ (g cm$^{-3}$) | $w_s$ (cm s$^{-1}$) | $w_b$ (cm s$^{-1}$) | %$_{swim}$ | $\theta_{V,swim}$ (deg) | $\theta_{V,dive}$ (deg) | $\|\vec{F}_{V,swim}\|$ (×10$^{-8}$ N) | $\|\vec{F}_{V,dive}\|$ (×10$^{-9}$ N) | $N_{obs}$ (×10$^{-5}$) |
|---|---|---|---|---|---|---|---|---|---|---|
| Control | 321±7.8 | 1.15±0.02 | –0.67±0.08 | –0.02±0.06 | 97.5±2.8 | 90.0±1.0 | –92.4±10.1 | 2.44±0.33 | 5.49±1.94 | 2.9±1.8 |
| Algae | 322±8.7 | 1.15±0.02 | –0.68±0.06 | –0.02±0.07 | 98.7±1.5 | 90.0±1.4 | –87.6±25.6 | 2.45±0.17 | 6.69±4.54 | 2.6±3.1 |
| Glass | 326±8.0 | 1.16±0.02 | –0.73±0.37 | 0.01±0.04 | 99.9±0.0 | 88.7±2.2 | –64.7±0.0 | 2.78±0.07 | 13.3±0.00 | 0.8±0.5 |
| Nylon | 323±4.8 | 1.15±0.01 | –0.71±0.25 | 0.08±0.09 | 100±0.0 | 89.6±3.1 | n.d. | 2.92±0.48 | n.d. | 0.3±0.2 |

$d$, larval shell length; $\rho_p$, larval density; $w_s$, terminal fall velocity of dead larvae; $w_b$, vertical velocity of swimming larvae; %$_{swim}$, percentage of larvae propelling themselves upward; $\theta_{V,swim}$ and $\theta_{V,dive}$, direction of upward and downward propulsion; $\|\vec{F}_{V,swim}\|$ and $\|\vec{F}_{V,dive}\|$, propulsive force magnitude of swimming and diving larvae; and $N_{obs}$, normalized number of observed tracks (no. tracks cm$^{-2}$ s$^{-1}$ larvae$^{-1}$).

Values are means ± 1 s.d. over all replicates per treatment, with nine control replicates and six replicates of each particle treatment. Notation n.d. indicates no data where no diving larvae were observed.

Table 2. Summary of flow statistics for turbulence treatments

| Level | $f$ (Hz) | $Re$ | $W$ (cm s$^{-1}$) | $w_{RMS}/u_{RMS}$ | ε (cm$^2$ s$^{-3}$) | $\eta_k$ (cm) | λ (cm) | $\Delta x$ (cm) |
|---|---|---|---|---|---|---|---|---|
| 0.2 | 0.02 | 36 | 0.04 | 1.64 | $4.5\times10^{-4}$ | 0.22 | 1.66 | 0.16 |
| 0.4 | 0.14 | 37 | 0.02 | 1.82 | $6.9\times10^{-4}$ | 0.20 | 1.40 | 0.16 |
| 0.6 | 0.25 | 121 | 0.13 | 1.45 | $3.6\times10^{-2}$ | 0.08 | 0.75 | 0.08 |
| 1.0 | 0.48 | 203 | 0.39 | 1.44 | $2.0\times10^{-1}$ | 0.05 | 0.53 | 0.08 |
| 2.0 | 1.04 | 461 | 0.52 | 1.45 | $8.6\times10^{-1}$ | 0.03 | 0.49 | 0.08 |
| 3.0 | 1.61 | 860 | 1.93 | 1.41 | $4.0\times10^{0}$ | 0.02 | 0.43 | 0.08 |

Level indicates turbulence tank setting; $f$, stirring frequency; $Re$, fluid Reynolds number; $W$, time- and space-averaged vertical velocity (positive upwards); $w_{RMS}/u_{RMS}$, isotropy ratio; ε, dissipation rate; $\eta_k$, Kolmogorov length scale; λ, Taylor microscale; and $\Delta x$, vector resolution.

860 (Table 2), where $Re=V_{RMS}\ell/\nu$, $V=(2u^2+w^2)^{0.5}$, the subscript RMS indicates a root mean square, $\ell=0.2z_o$, and $\ell$ is the eddy length scale at a distance $z_o$ from the grids. The spatially averaged dissipation rates were $\varepsilon=4.5\times10^{-4}$ to 4.0 cm$^2$ s$^{-3}$, with corresponding Kolmogorov length scales of $\eta_k=0.22$–0.02 cm. The characteristic eddy length scale can be estimated by the Taylor microscale $\lambda=(15\nu V_{RMS}^2/\varepsilon)^{0.5}$ and ranged from 0.43 to 1.66 cm. To obtain highly accurate dissipation rate estimates, the vector resolution $\Delta x$ should be close to the Kolmogorov length scale ($1\leq\Delta x/\eta<3$) and less than 30% of the Taylor microscale λ (Antonia et al., 1994; Saarenrinne and Piirto, 2000; Tanaka and Eaton, 2007; de Jong et al., 2009). Here, $\Delta x/\eta$ ranged from 0.73 to 4.0 and $\Delta x$ was 10–19% of λ. Based on the $\Delta x/\eta$ criterion, ε may have been underestimated by up to ~10% at the highest turbulence level (Antonia et al., 1994). These errors are negligible for the behavior analysis given that measured dissipation rates spanned four orders of magnitude. Mean flows were upward, and turbulence was relatively anisotropic with isotropy ratios of $w_{RMS}/u_{RMS}=1.41$–1.64. This deviation from isotropy indicates the presence of weak secondary flows and was an unavoidable consequence of making measurements away from the center of the tank.

### Larval behavior in turbulence

The apparent range of larval vertical behavioral velocities varied with the turbulence characteristic used for binning (Fig. 2). Average larval velocities $w_b$ were always slightly above zero in weaker turbulence and then became increasingly negative in turbulence above a threshold level. The average descent speed was about one-third higher when larval velocity was binned by acceleration or dissipation rate than when it was binned by strain rate or vorticity, indicating that rapid descents were most strongly associated with high accelerations and high dissipation rates. Based on the range of average velocities, the variation in $w_b$ was best explained by dissipation rate, followed by acceleration, vorticity and strain rate. The fitted behavior model (Eqn 5) also gave the highest coefficient of determination for dissipation rate, followed by acceleration, vorticity and strain rate (Table 3). Estimates from Eqn 5 indicate that larval velocities switched from positive to negative at threshold values of $\alpha_{cr}=3.78\times10^{-1}$ cm s$^{-2}$, $\gamma_{cr}=1.34\times10^{-1}$ s$^{-1}$, $\xi_{cr}=3.64\times10^{-1}$ s$^{-1}$ and $\varepsilon_{cr}=7.78\times10^{-2}$ cm$^2$ s$^{-3}$.

The force balance analysis demonstrated patterns in the direction and magnitude of propulsive force as a response to turbulence. The fraction of larvae propelling themselves downward was strongly dependent on turbulence (Fig. 3). The fractions of swimmers and divers changed most abruptly when larvae were averaged in small bins of acceleration, with a sudden change of slope corresponding to the threshold acceleration $\alpha_{cr}$. The fractions of swimmers and divers changed more gradually when larvae were binned by strain rate, vorticity or dissipation rate. The classification of larvae as swimmers or divers was generally insensitive to $L$. Although the

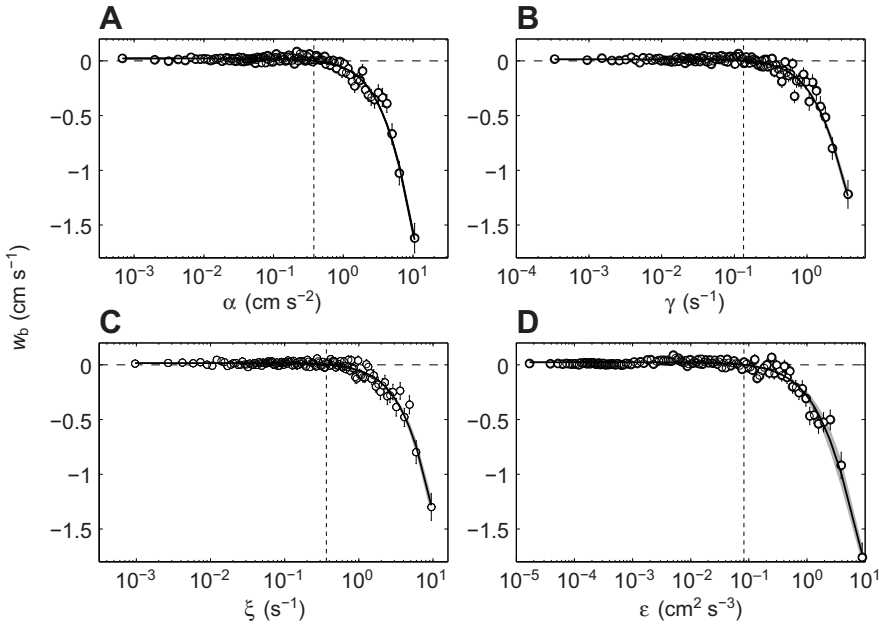


Fig. 2. Model fit to larval vertical behavioral velocity $w_b$ as a function of turbulence statistics. (A) Acceleration α ($R^2$=0.96), (B) strain rate γ ($R^2$=0.94), (C) vorticity ξ ($R^2$=0.94) and (D) dissipation rate ε ($R^2$=0.97). Circles and error bars are mean (±1 s.e.m.) behavioral velocities for individual larvae grouped in small bins of α, γ, ξ or ε. Solid black line is the fitted behavior model (Eqn 5), shaded area is a 95% prediction interval, horizontal dashed line indicates neutral buoyancy ($w_b$=0) and vertical dashed line indicates critical values of $\alpha_{cr}$, $\gamma_{cr}$, $\xi_{cr}$ or $\varepsilon_{cr}$ from Table 3.

Table 3. Summary of fitted behavior model (Eqn 5) describing larval behavioral vertical velocity $w_b$ as a function of acceleration α, strain rate γ, vorticity ξ or dissipation rate ε

| Statistic (**x** units) | $\hat{b}_0$ (cm s$^{-1}$) | $\hat{b}_1$ (cm s$^{-1}$) | $\hat{b}_2$ | $\hat{b}_3$ | $\mathbf{x}_{cr}$ (**x** units) | $R^2$ |
|---|---|---|---|---|---|---|
| α (cm s$^{-2}$) | 0.021 | –4.52 | 52.98 | 1.45 | $3.78\times10^{-1}$ | 0.96 |
| γ (s$^{-1}$) | 0.014 | –2.99 | 9.97 | 1.51 | $1.34\times10^{-1}$ | 0.94 |
| ξ (s$^{-1}$) | 0.016 | –4.60 | 66.69 | 1.45 | $3.64\times10^{-1}$ | 0.94 |
| ε (cm$^2$ s$^{-3}$) | 0.023 | –3.66 | 10.80 | 1.05 | $7.78\times10^{-2}$ | 0.97 |

Values given are parameters $\hat{b}_0$, $\hat{b}_1$, $\hat{b}_2$ and $\hat{b}_3$, where hats indicate estimates from non-linear regression of Eqn 5, critical values $\mathbf{x}_{cr}$, and coefficient of determination $R^2$ for fitted Eqn 5.

rotation angle ϕ varied widely with $L$, the propulsion angle $\theta_V$ varied little (Fig. 4), and larvae rarely experienced both a large ϕ and a large $\theta_V$ simultaneously.

All larvae experienced a larger average rotation angle ϕ in stronger turbulence because of increasing vorticity, but the average direction of propulsion $\theta_V$ relative to the larval axis remained steady (Fig. 4). For divers, ϕ at low dissipation rates (Fig. 4A) was generally smaller and less variable than ϕ at low accelerations (Fig. 4B) or strain rates (not shown). This inconsistency may arise because the rotation angle is defined by vorticity, which is more strongly correlated with dissipation rate than with acceleration or strain rate. In larval coordinates, the propulsive force was consistently directed at an average angle of $\theta_V\approx90$ deg for swimmers and $\theta_V\approx-90$ deg for divers (Fig. 4C,D), although $\theta_V$ for divers was variable in weak turbulence where diving was infrequent.

Both swimmers and divers used more propulsive force $\|\vec{F}_V\|$ and had higher behavioral velocity magnitudes $|w_b|$ in stronger turbulence (Fig. 5). Swimmers directed their propulsive force upward and showed a steady rise in $\|\vec{F}_V\|$ with turbulence, so their vertical velocities increased from near zero in calm water to $w_b\approx0.5$ cm s$^{-1}$ in intermediate turbulence. Despite the steady rise in propulsive force, swimmers' velocities leveled off and even dropped in strong turbulence, presumably because larvae rotated and their propulsive force was directed away from vertical. Diving larvae had a more complex response to turbulence. In weaker turbulence, $\|\vec{F}_V\|$ and $w_b$ grew steadily with turbulence when larvae were binned by ε but were extremely variable when larvae were binned by α, γ and ξ. At low ε the diving velocities were near the estimated terminal fall velocity ($w_s$=–0.58±0.11 cm s$^{-1}$). In stronger turbulence, $\|\vec{F}_V\|$ and $|w_b|$ of divers grew steadily with turbulence regardless of which characteristic was used for binning. At the highest ε the diving velocities reached $w_b\approx-3$ cm s$^{-1}$, five times the terminal fall velocity of passive larvae. The variation in propulsive force and velocity of larval dives was best explained by dissipation rate, particularly in weaker turbulence.

The apparent dependence of behavioral velocity and propulsive force on dissipation rate was further supported by the relationships between $\|\vec{F}_V\|$ or $w_b$ and the rotation angle ϕ (Fig. 6). When larvae were grouped in small bins of dissipation rate, the propulsive forces and diving velocities were highly correlated with the larval rotation angle ($R^2\geq0.93$ for linear regressions). For swimmers, the relationship between $w_b$ and ϕ appeared more non-linear because at large rotation angles ($|\phi|>10$ deg) the larval propulsive force was directed away from the positive $z$ direction. The relationships between $w_b$ or $\|\vec{F}_V\|$ and ϕ were weaker when larvae were binned by acceleration or strain rate and weakest when larvae were binned by vorticity ξ, even though rotation angle was estimated directly from vorticity. This result implies that the strength of a diving reaction depends less on axial rotation than on more general features of small-scale turbulence.

## DISCUSSION

The observed behaviors of oyster larvae provide intriguing new insights into how and why larvae respond to turbulence. The use

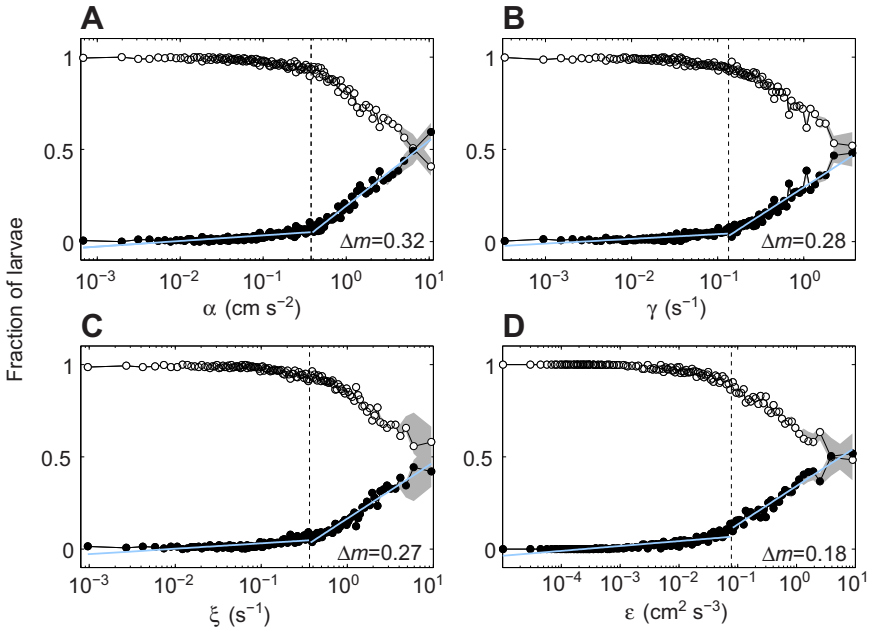


Fig. 3. Fractions of larvae *versus* (A) acceleration α, (B) strain rate γ, (C) vorticity ξ and (D) dissipation rate ε for larvae propelling themselves upward (swimmers; open circles) and downward (divers; filled circles) relative to the larval axis. Circles are fractions of larvae in small bins of α, γ, ξ or ε with the distance between centers of gravity and buoyancy $L$=3 μm; shaded areas indicate the range of estimates for $L$=1.5–6 μm, and dashed lines indicate critical values of $\alpha_{cr}$, $\gamma_{cr}$, $\xi_{cr}$ or $\varepsilon_{cr}$ from Table 3. Light blue lines are linear regressions of the fraction of diving larvae *versus* $\log_{10}$ of α, γ, ξ or ε above and below the critical values, and $\Delta m$ is the difference in slopes above and below the critical values.

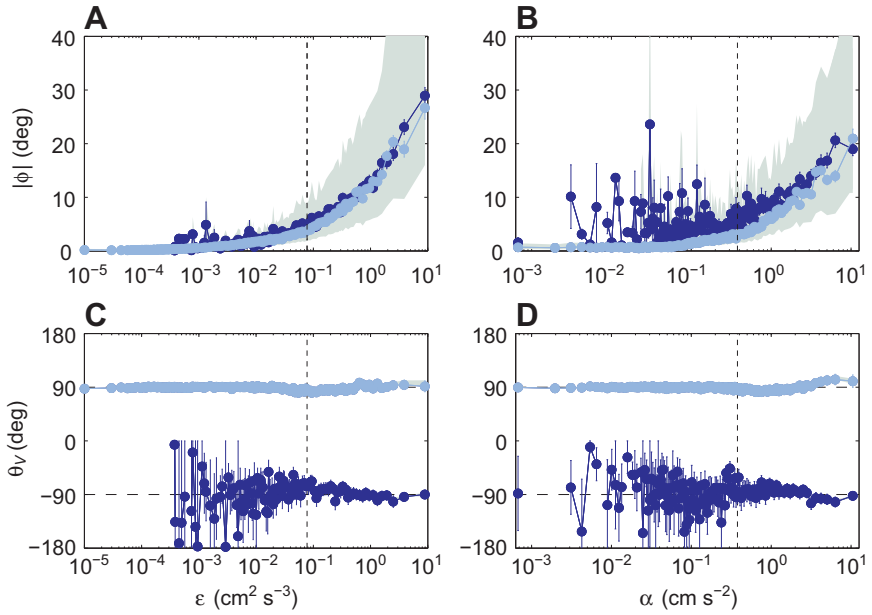


Fig. 4. Angles of larval axial rotation |ϕ| (A,B) and propulsion $\theta_V$ (C,D) *versus* dissipation rate ε (A,C) and acceleration α (B,D) for larvae propelling themselves upward (swimmers; light blue circles) and downward (divers; dark blue circles) relative to the larval axis. Circles and error bars are means (±1 s.e.m.) of estimates grouped over small bins of ε or α with $L$=3 µm, shaded areas indicate the range of estimates for $L$=1.5–6 µm, vertical dashed lines indicate threshold values of $\varepsilon_{cr}$ or $\alpha_{cr}$ from Table 3 and horizontal dashed lines in C and D indicate directions ($\theta_V$) of ±90 deg.

of IR PIV enabled us to measure simultaneously the behavioral velocities and propulsive forces of individual larvae as a response to instantaneous turbulence. Like other veligers (Fuchs et al., 2004; Fuchs and DiBacco, 2011), oyster larvae frequently descended in strong turbulence. Unlike other veligers, however, oyster larvae reached descent velocities that greatly exceeded the terminal fall velocity of passive larvae (Fig. 7A). Our results suggest that oyster larvae undergo a behavioral shift from infrequent, nearly passive descents in weaker turbulence to frequent, active dives in stronger turbulence. Active diving has little precedent among invertebrate larvae. Diving would require an energy expenditure and is an exciting contrast to previous observations of mollusc larvae that sink passively by retracting the velum. If oysters have developed energetically demanding strategies to achieve high diving speeds, this implies that there is strong selective pressure for larvae to descend in turbulent environments.

Before discussing the implications of active diving, we first address whether the observed descent speeds could arise solely from turbulence-enhanced passive sinking (e.g. Ruiz et al., 2004). Passive larvae could have different average sinking speeds in turbulence than in still water if the larvae have inertia. Inertia is negligible for passive particles at particle Reynolds numbers of $Re_p$<0.5, and at low $Re_p$ the average terminal velocity is unaffected by turbulence (Reeks, 1977). At $Re_p$>0.5 particles gain inertia, and the average sinking velocity can be lower or higher in turbulence than in still water. Oyster larvae would have $Re_p$=1.7 when sinking passively at the terminal velocity. The larvae observed in turbulence had $Re_p$ up to 8.8 on average and up to 25.7 for individual larvae (Fig. 7B). Given these intermediate particle Reynolds numbers, we must consider whether larval inertia contributed to higher sinking velocities in turbulence.

### Scales of larvae and turbulence

For inertial particles, turbulence has the greatest effect on particle velocity when particle velocity is similar to the Kolmogorov velocity scale, $w_s/\upsilon_k \approx 1$, when particle size differs from the Kolmogorov length scale, $d/\eta_k \neq 1$, and when the particle response time $\tau_p = d^2\rho_p(18\nu\rho_f)^{-1}$ is similar to the Kolmogorov time scale, giving a Stokes number of $St = \tau_p/\tau_k \approx 1$ (e.g. Wang and Maxey, 1993). Terminal velocity can also be reduced by added drag on non-spherical shapes, but the effects of shape are small at $Re_p$<10 (Komar and Reimers, 1978; Davies, 1979). For passive sinkers, the terminal fall velocity was comparable to the Kolmogorov velocity scale in the strongest turbulence, with $w_s/\upsilon_k \approx 1$ at ε=10 cm$^2$ s$^{-3}$ (Fig. 7B). For observed larvae, the velocity-scale ratios were always greater than one, with $\|\vec{V}_b\|/\upsilon_k$=2.6–6.1 for swimmers and 5.9–17.2 for divers. Thus, by the velocity criterion, turbulence may have sped up the descent of passively sinking larvae, although the observed larvae were less likely to experience the same effect.

By the size and time scale criteria, in contrast, turbulence could have slowed or had no effect on larval descent (Fig. 7B). Inertial particles that are smaller than $\eta_k$ tend to concentrate in high-strain-rate, low-vorticity regions and can have terminal velocities 27–50% higher in turbulence than in still water (Maxey, 1987; Wang and Maxey, 1993), whereas particles larger than $\eta_k$ experience more drag and have lower terminal velocities in turbulence than in still water (e.g. Brucato et al., 1998). Oyster larvae were smaller than $\eta_k$ at low dissipation rates and slightly larger than $\eta_k$ at ε≥1 cm$^2$ s$^{-3}$ (Fig. 7B). The ratio of length scales was too close to $d/\eta_k$=1 at ε>$\varepsilon_{cr}$ to expect much effect of turbulence on descent velocities (Wang and Maxey, 1993; Brucato et al., 1998), but by the size criterion the strongest turbulence may have slowed the larval descents. Larval response times were also too short to expect much effect of turbulence on descent velocities. Larval Stokes numbers were generally $St$<<1, reaching only $St$≈0.01 at the threshold dissipation rate and $St$≈0.1 at the highest dissipation rate (Fig. 7B). These low Stokes numbers indicate that larvae had short response times and would be unlikely to form clusters or experience a downward bias in turbulent transport (Salazar et al., 2008).

Based on these considerations of scale, the potential effects of turbulence on descent speeds were inconsistent. Turbulence was unlikely to greatly speed larval descent, and we are confident that the observed descents were active dives rather than turbulence-enhanced passive sinking. Even if we assume that turbulence raised larval descent speeds by the maximum amount (50%) (Wang and Maxey, 1993), the observed descents in strong turbulence could not be explained by passive sinking (Fig. 7A), indicating that larvae actively propelled themselves downward.

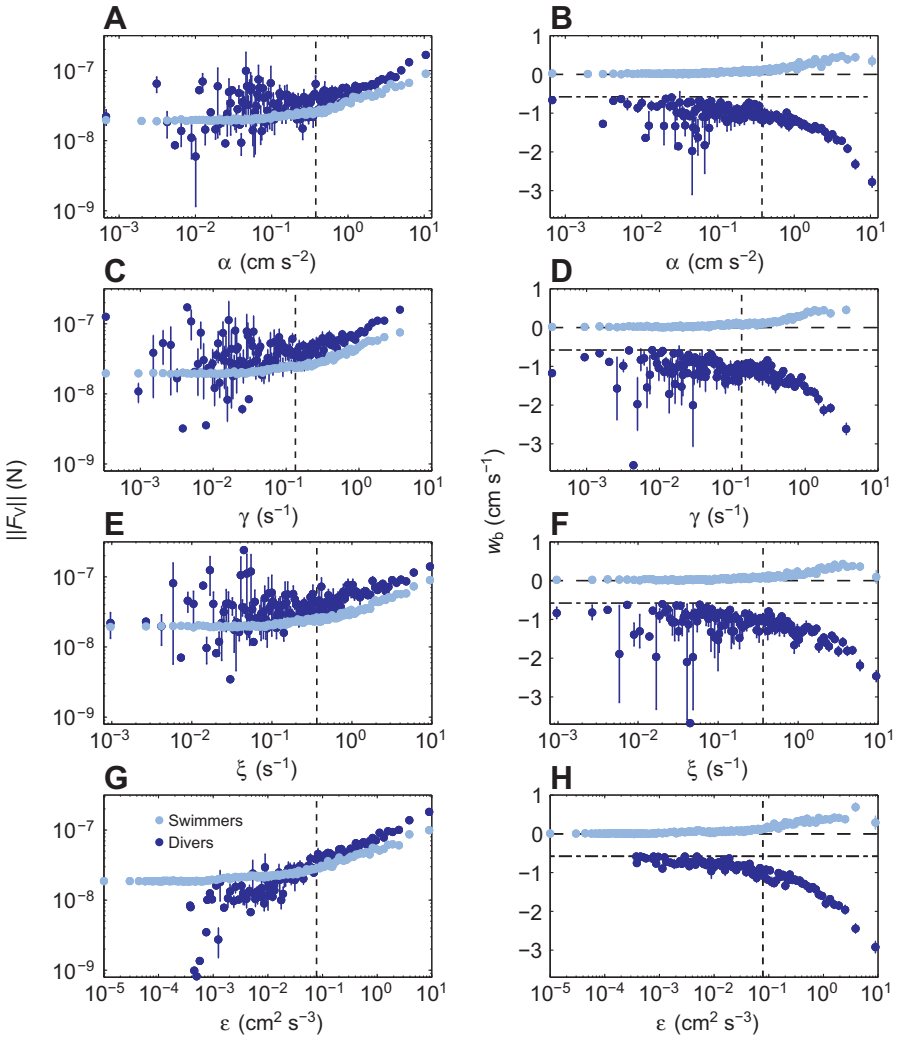


Fig. 5. Larval propulsive force magnitude $\|\vec{F}_V\|$ and behavioral vertical velocity $w_b$ *versus* (A,B) acceleration α, (C,D) strain rate γ, (E,F) vorticity ξ and (G,H) dissipation rate ε for larvae propelling themselves upward (swimmers; light blue circles) and downward (divers; dark blue circles) relative to the larval axis. Circles and error bars are means (±1 s.e.m.) of estimates grouped over small bins of α, γ, ξ or ε with $L$=3 μm, vertical dashed lines indicate threshold values of $\alpha_{cr}$, $\gamma_{cr}$, $\xi_{cr}$ or $\varepsilon_{cr}$ from Table 3, horizontal dashed lines indicate neutral buoyancy $w_b$=0, and dash-dotted lines indicate terminal fall velocity $w_b$=$w_s$.

### Larval propulsion

Our results provide compelling evidence that larvae dove more frequently and more forcefully in stronger turbulence. Even in still water the propulsive force used for swimming exceeded estimates for other ciliated larvae ($\|\vec{F}_V\|$=0.5×10$^{-9}$ to 5.8×10$^{-9}$ N) (Jonsson et al., 1991; Emlet, 1994; Hansen et al., 2010) because oyster veligers are larger or more dense than larvae studied previously. In turbulence, the propulsive force and behavioral velocity magnitudes of both swimming and diving larvae grew steadily with dissipation rate. A similar turbulence-induced increase in swimming activity was observed in ciliated echinoid blastulae (*Dendraster excentricus*), which swam faster in stronger shear (McDonald, 2012). Swimming oyster larvae reached ascent velocities of only a few millimeters per second, because although they used more upward propulsive force in stronger turbulence, they also experienced larger axial rotation angles that directed the propulsive force away from vertical. This rotation-induced limitation of larval swimming abilities is consistent with model predictions for larvae that lose their passively stable orientation in shearing flow (Grünbaum and Strathmann, 2003; Clay and Grünbaum, 2010). Diving larvae also experienced large rotation angles in strong turbulence, but they compensated for rotation by using more propulsive force than swimmers and achieved impressive descent speeds of up to a few centimeters per second.

The observed behavioral shift from nearly passive sinking to active diving may require a change in propulsive mode. Mollusc veligers propel themselves by beating the velar cilia, with propulsive forces directed upward relative to the larval axis. A faster ciliary beat generates more propulsive force and a higher upward swimming velocity (Arkett et al., 1987; Gallager, 1993). Descent generally requires less energy than ascent because veligers are denser than water and can descend by slowing the ciliary beat, arresting the cilia or drawing the velum inside the shell (Arkett et al., 1987; Gallager, 1993). Some ciliated larvae can reverse their swimming direction by reversing the direction of ciliary beat (e.g. Lacalli and Gilmour, 1990), but we are unaware of any reports of ciliary reversal in veligers. Without a ciliary reversal it is implausible that diving larvae generated the observed propulsive forces or diving speeds by ciliary swimming alone.

Larvae potentially gained some additional downward thrust by another propulsive mechanism such as flapping the lobes of the velum. Flapping is a common swimming mode among planktonic molluscs. Pteropods flap their parapodia and can do so both as larvae before losing the velum or as adults in alternation with ciliary swimming (Bandel and Hemleben, 1995; Childress and Dudley, 2004; Borrell et al., 2005). Some snail veligers have been observed flapping the velum, although observations are limited to larvae with intermediate particle Reynolds numbers of $Re_p$≈4–10 (H.L.F., unpublished observation) (Lebour, 1931; Manríquez and Castilla, 2011). Flapping of appendages can generate positive thrust even at low particle Reynolds numbers and becomes energetically efficient

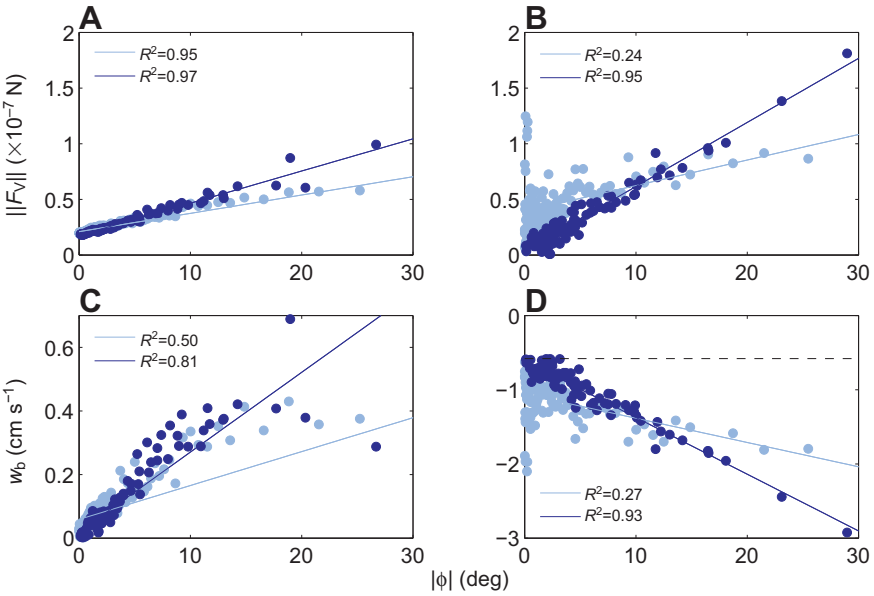


Fig. 6. Average larval (A,B) behavioral vertical velocity $w_b$ and (C,D) propulsive force magnitude ||$\vec{F}_V$|| *versus* axial rotation angle |ϕ| for larvae propelling themselves upward (A,C; swimmers) and downward (B,D; divers) relative to the larval axis. Circles are means for larvae grouped in small bins of dissipation rate (ξ, dark blue) or vorticity (ε, light blue), solid lines are linear regressions and the dashed line in D indicates terminal fall velocity.

at $Re_p$=5–20 (Walker, 2002; Childress and Dudley, 2004). In this study, some larvae certainly experienced the range of $Re_p$ where flapping would become an energetically efficient mode of propulsion.

### Responses to velocity gradients

We expected larvae to change their behavior in response to spatial or temporal velocity gradients, but no gradients emerged as a dominant behavioral cue. In our experiments the velocity gradients were correlated with one another, and their effects on behavior could not be completely isolated. Yet, we found little evidence of abrupt behavioral changes at threshold values of any velocity gradients. One exception was the fraction of diving larvae, which underwent a larger change in slope at the threshold acceleration $\alpha_{cr}$ than at $\gamma_{cr}$, $\xi_{cr}$ or $\varepsilon_{cr}$ (Fig. 3). Stronger dives were also more closely associated with high accelerations than with high spatial gradients. Overall, however, the strength of a dive appeared most related to dissipation rate, and in weak turbulence the strength of a dive showed no relationship with any turbulence characteristic except dissipation rate. These results suggest that larval dives are a complex reaction to multiple aspects of small-scale turbulence.

Based on the larval responses to turbulence, we suspect that the statocysts may be more important than the velar cilia for turbulence detection. Statocysts could detect accelerations when the statolith is accelerated into the mechanosensory cilia lining the statocyst lumen. The threshold value $\alpha_{cr}$ was associated with an increase in diving frequency and may correspond to an acceleration at which the statolith impacts the cilia with enough force to deflect them by a threshold amount. The statocysts could also detect axial rotation due to vorticity as the statoliths rolled onto cilia around the internal surface (e.g. Gallin and Wiederhold, 1977). The rotation angle had no obvious influence on whether larvae swam or dove but did explain most of the variation in propulsive force, particularly by diving larvae. Statocysts probably play a role in both detecting and responding to turbulence.

Whereas statocysts would detect acceleration or rotation of the larval body, cilia could detect spatial gradients such as strain rate in the surrounding fluid. The ability of larvae to detect strain rate depends on the size of the detector, so it is useful to convert strain rate to a signal strength $d\gamma$, where $d$ is an appropriate length scale. The threshold strain rate for oyster larvae gives a signal strength of $d\gamma_{cr}\approx4\times10^{-3}$ cm s$^{-1}$ over the length of a larva. This threshold is 10–100 times lower than signal strengths inducing jumps in the most sensitive copepods (0.02 cm s$^{-2}$) (Kiørboe et al., 1999) and

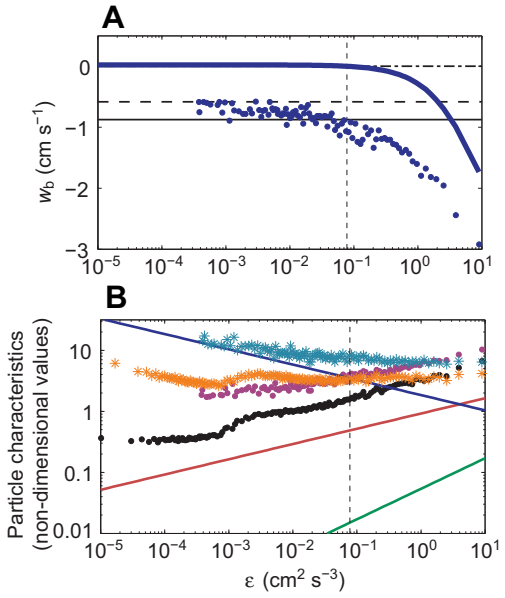


Fig. 7. Average larval (A) behavioral velocities and (B) particle characteristics *versus* dissipation rate ε. Behavioral velocities (A) are shown in blue as a fitted model of average behavioral vertical velocity $w_b$ for all larvae (Eqn 5; thick blue line) and measured $w_b$ for divers only (circles). Black lines indicate reference values: neutral buoyancy $w_b$=0 (dash-dotted line), the expected velocity for larvae sinking passively in still water, $w_b$=$w_s$ (Eqn 15; horizontal dashed line), and the expected limit of velocity for larvae sinking passively with turbulence-enhanced sinking, $w_b$=1.5$w_s$ (solid line). Particle characteristics (B) include particle Reynolds number $Re_p$=$d$||$\vec{V}_b$||/ν of swimmers (black circles) and divers (purple circles), Stokes number $St$ ($\tau_p/\tau_k$; green line), ratio of larval length to Kolmogorov length scale $d/\eta_k$ (red line), ratio of larval terminal velocity to Kolmogorov velocity scale |$w_s$|/$\upsilon_k$ (blue line), and ratio of observed larval velocity to Kolmogorov velocity scale ||$\vec{V}_b$||/$\upsilon_k$ for swimmers (orange stars) and divers (cyan stars). Vertical dashed lines in A and B indicate the threshold dissipation rate $\varepsilon_{cr}$.

comparable to signal strengths inducing jumps in the most sensitive ciliates and flagellates ($3.1\times10^{-3}$ cm s$^{-2}$) (Jakobsen, 2001). If we assume a cilium length of $d_c \leq 50$ μm (e.g. Sleigh and Blake, 1977), the threshold signal strength over a cilium is $d_c\gamma_{cr} < 7\times10^{-4}$ cm s$^{-1}$, lower than any threshold previously observed. The estimated threshold signal strengths are improbably low, and the larvae exhibited no abrupt behavioral changes at those thresholds, so it is unlikely that velar cilia are solely responsible for sensing turbulence.

### Ecological implications

Oyster larvae exhibited an extraordinary diving behavior that would enable them to rapidly approach the seabed. Rapid descents may confer large fitness gains because unlike most shallow-water species, oysters form discrete reefs on intertidal or subtidal mud flats. These reefs are patchy, tens to hundreds of meters long, and rougher than surrounding substrates. Natural oyster reefs have drag coefficients of $C_d \approx 0.11$ (Whitman and Reidenbach, 2012), 10–100 times greater than those over flat mud or sand (e.g. Green et al., 1998; Geyer et al., 2000; Whitman and Reidenbach, 2012). Drag coefficients are related to shear velocity $u_*$ by the quadratic drag law, $u_* = C_d^{0.5} U$, and dissipation rate can be estimated as $\varepsilon = u_*^3/\kappa z$, where $\kappa = 0.41$ is von Karman's constant. Based on these simple models and observed drag coefficients, the dissipation rates should also be 10–100 times higher over oyster reefs than over surrounding mud flats. Larvae that respond to high dissipation rates by descending would be more likely to concentrate near the bed over a reef than over the flats. Descent speed may be critical in determining whether larvae contact a reef patch before passing over onto flatter substrates. Larvae would have better odds of hitting an oyster reef if they dive actively than if they sink passively, and the improved settlement odds may confer fitness benefits that offset the energetic cost of active downward propulsion. Settlement rates could be further enhanced by responses to chemical cues near the bed (e.g. Turner et al., 1994; Koehl and Reidenbach, 2007). Using a numerical model that will be presented elsewhere, we are investigating how larval behaviors interact with substrate type to affect oyster settlement.

## LIST OF SYMBOLS

| | |
|---|---|
| $d$, $r$ | larval shell length and radius |
| $\vec{F}_A$ | added mass or acceleration reaction force vector |
| $\vec{F}_B$ | Basset or Boussinesq force vector |
| $\vec{F}_D$ | viscous Stokes drag force vector |
| $\vec{F}_F$ | form drag force vector |
| $\vec{F}_P$ | pressure gradient force vector |
| $\vec{F}_V$ | velar propulsion force vector |
| $\vec{F}_W$ | weight force vector |
| $\vec{g}$ | acceleration due to gravity |
| $L$ | distance between centers of buoyancy and gravity |
| $m$ | larval mass |
| $Re$ | fluid Reynolds number |
| $Re_p$ | particle Reynolds number |
| $St$ | Stokes number |
| $u$, $w$ | vertical and horizontal fluid velocity |
| $u_b$, $w_b$ | vertical and horizontal larval behavioral velocity |
| $u_o$, $w_o$ | vertical and horizontal observed larval velocity |
| $\vec{V}_b$ | behavioral component of larval translational velocity vector |
| $\vec{V}_f$ | fluid component of larval translational velocity vector |
| $\vec{V}_o$ | observed larval translational velocity vector |
| $w_s$ | larval terminal sinking velocity |
| $\alpha$ | fluid acceleration |
| $\gamma$ | strain rate |
| $\varepsilon$ | kinetic energy dissipation rate |
| $\xi$ | horizontal component of vorticity |
| $\eta_k$ | Kolmogorov length scale |
| $\theta_V$ | angle of larval propulsion relative to larval axis |
| $\kappa$ | von Karmann's constant (=0.41) |
| $\mu$ | dynamic viscosity |
| $\nu$ | kinematic viscosity (=0.01 cm$^2$ s$^{-1}$) |
| $\upsilon_k$ | Kolmogorov velocity scale |
| $\rho_f$ | fluid density |
| $\rho_p$ | particle density |
| $\tau_k$ | Kolmogorov time scale |
| $\tau_p$ | particle response time |
| $\phi$ | angle of larval axial rotation due to shear |


## ACKNOWLEDGEMENTS

We thank D. Merritt and S. Alexander at Horn Point Laboratory for providing the oyster larvae. G. Gerbi, F. J. Diez, A. Christman, K. Helfrich and L. Mullineaux contributed to helpful discussions, and G. Gerbi, J. P. Grassle and two anonymous reviewers provided constructive comments on the manuscript.

## AUTHOR CONTRIBUTIONS

H.L.F. contributed to all aspects of the research, E.J.H. contributed to data analysis and writing, E.L.S. contributed to data collection, and R.A.G. contributed to data analysis and editing.

## COMPETING INTERESTS

No competing interests declared.

## FUNDING

This research was supported by the National Science Foundation (NSF) [grant no. OCE-1060622 to H.L.F.]. E.L.S. was supported by a Research Internship in Ocean Sciences [NSF grant no. OCE-1062894 to G. Taghon].


## REFERENCES


**Adrian, R. J.** (1991). Particle-imaging techniques for experimental fluid mechanics. *Annu. Rev. Fluid Mech.* **23**, 261-304.

**Adrian, R. J.** (1997). Dynamic ranges of velocity and spatial resolution of particle image velocimetry. *Meas. Sci. Technol.* **8**, 1393-1398.

**Antonia, R. A., Zhu, Y. and Kim, J.** (1994). Corrections for spatial velocity derivatives in a turbulent shear flow. *Exp. Fluids* **16**, 411-413.

**Arkett, S. A., Mackie, G. O. and Singla, C. L.** (1987). Neuronal control of ciliary locomotion in a gastropod veliger (*Calliostoma*). *Biol. Bull.* **173**, 513-526.

**Armenio, V. and Fiorotto, V.** (2001). The importance of forces acting on particles in turbulent flows. *Phys. Fluids* **13**, 2437-2440.

**Bandel, K. and Hemleben, C.** (1995). Observations on the ontogeny of thecosomatous pteropods (holoplanktonic Gastropoda) in the southern Red Sea and from Bermuda. *Mar. Biol.* **124**, 225-243.

**Barile, P. J., Stoner, A. W. and Young, C. M.** (1994). Phototaxis and vertical migration of the queen conch (*Strombus gigas linne*) veliger larvae. *J. Exp. Mar. Biol. Ecol.* **183**, 147-162.

**Borrell, B. J., Goldbogen, J. A. and Dudley, R.** (2005). Aquatic wing flapping at low Reynolds numbers: swimming kinematics of the Antarctic pteropod, *Clione antarctica*. *J. Exp. Biol.* **208**, 2939-2949.

**Brucato, A., Grisafi, F. and Montante, G.** (1998). Particle drag coefficients in turbulent fluids. *Chem. Eng. Sci.* **53**, 3295-3314.

**Brumley, B. H. and Jirka, G. H.** (1987). Near-surface turbulence in a grid-stirred tank. *J. Fluid Mech.* **183**, 235-263.

**Catton, K. B., Webster, D. R., Brown, J. and Yen, J.** (2007). Quantitative analysis of tethered and free-swimming copepodid flow fields. *J. Exp. Biol.* **210**, 299-310.

**Cheng, Y., Pothos, S. and Diez, F. J.** (2010). Phase discrimination method for simultaneous two-phase separation in time-resolved stereo PIV measurements. *Exp. Fluids* **49**, 1375-1391.

**Chia, F. S., Koss, R. and Bickell, L. R.** (1981). Fine structural study of the statocysts in the veliger larva of the nudibranch, *Rostanga pulchra*. *Cell Tissue Res.* **214**, 67-80.

**Childress, S. and Dudley, R.** (2004). Transition from ciliary to flapping mode in a swimming mollusc: flapping flight as a bifurcation in $Re_\omega$. *J. Fluid Mech.* **498**, 257-288.

**Clay, T. W. and Grünbaum, D.** (2010). Morphology-flow interactions lead to stage-selective vertical transport of larval sand dollars in shear flow. *J. Exp. Biol.* **213**, 1281-1292.

**Cragg, S. M.** (1980). Swimming behaviour of the larvae of *Pecten maximus* (L.) (Bivalvia). *J. Mar. Biol. Assoc. UK* **60**, 551-564.

**Davies, C. N.** (1979). Particle-fluid interaction. *J. Aerosol Sci.* **10**, 477-513.

**de Jong, J., Cao, L., Woodward, S. H., Salazar, J. P. L. C., Collins, L. R. and Meng, H.** (2009). Dissipation rate estimation from PIV in zero-mean isotropic turbulence. *Exp. Fluids* **46**, 499-515.

**Dickinson, A. J. G.** (2002). Neural and muscular development in a gastropod larva. PhD dissertation, Dalhousie University, Nova Scotia, Canada.

**Emlet, R. B.** (1994). Body form and patterns of ciliation in nonfeeding larvae of echinoderms: functional solutions to swimming in the plankton? *Am. Zool.* **34**, 570-585.

**Finelli, C. M. and Wethey, D. M.** (2003). Behavior of oyster (*Crassostrea virginica*) larvae in flume boundary layer flows. *Mar. Biol.* **143**, 703-711.

**Fretter, V.** (1967). The prosobranch veliger. *J. Molluscan Stud.* **37**, 357-366.
**Fuchs, H. L. and DiBacco, C.** (2011). Mussel larval responses to turbulence are unaltered by larval age or light conditions. *Limnol. Oceanogr. Fluid Environ.* **1**, 120-134.
**Fuchs, H. L., Mullineaux, L. S. and Solow, A. R.** (2004). Sinking behavior of gastropod larvae (*Ilyanassa obsoleta*) in turbulence. *Limnol. Oceanogr.* **49**, 1937-1948.
**Fuchs, H. L., Neubert, M. G. and Mullineaux, L. S.** (2007). Effects of turbulence-mediated larval behavior on larval supply and settlement in tidal currents. *Limnol. Oceanogr.* **52**, 1156-1165.
**Fuchs, H. L., Solow, A. R. and Mullineaux, L. S.** (2010). Larval responses to turbulence and temperature in a tidal inlet: habitat selection by dispersing gastropods? *J. Mar. Res.* **68**, 153-188.
**Gallager, S. M.** (1993). Hydrodynamic disturbances produced by small zooplankton: case study for the veliger larva of a bivalve mollusc. *J. Plankton Res.* **15**, 1277-1296.
**Gallin, E. K. and Wiederhold, M. L.** (1977). Response of *Aplysia* statocyst receptor cells to physiologic stimulation. *J. Physiol.* **266**, 123-137.
**George, W. K. and Hussein, H. J.** (1991). Locally axisymmetric turbulence. *J. Fluid Mech.* **233**, 1-23.
**Geyer, W. R., Trowbridge, J. H. and Bowen, M. M.** (2000). The dynamics of a partially mixed estuary. *J. Phys. Oceanogr.* **30**, 2035-2048.
**Gibbs, R. J., Matthews, M. D. and Link, D. A.** (1971). The relationship between sphere size and settling velocity. *J. Sediment. Petrol.* **41**, 7-18.
**Green, M. O., Hewitt, J. E. and Thrush, S. F.** (1998). Seabed drag coefficient over natural beds of horse mussels (*Atrina zelandica*). *J. Mar. Res.* **56**, 613-637.
**Grünbaum, D. and Strathmann, R. R.** (2003). Form, performance and trade-offs in swimming and stability of armed larvae. *J. Mar. Res.* **61**, 659-691.
**Guo, J.** (2011). Motion of spheres falling through fluids. *J. Hydraul. Eng.* **49**, 32-41.
**Hadfield, M. G. and Koehl, M. A. R.** (2004). Rapid behavioral responses of an invertebrate larva to dissolved settlement cue. *Biol. Bull.* **207**, 28-43.
**Hansen, B. W., Jakobsen, H. H., Andersen, A., Almeda, R., Pedersen, T. M., Christensen, A. M. and Nilsson, B.** (2010). Swimming behavior and prey retention of the polychaete larvae *Polydora ciliata* (Johnston). *J. Exp. Biol.* **213**, 3237-3246.
**Hopfinger, E. J. and Toly, J.-A.** (1976). Spatially decaying turbulence and its relation to mixing across density interfaces. *J. Fluid Mech.* **78**, 155-175.
**Jakobsen, H. H.** (2001). Escape response of planktonic protists to fluid mechanical signals. *Mar. Ecol. Prog. Ser.* **214**, 67-78.
**Jonsson, P. R., André, C. and Lindegarth, M.** (1991). Swimming behaviour of marine bivalve larvae in a flume boundary-layer flow: evidence for near-bottom confinement. *Mar. Ecol. Prog. Ser.* **79**, 67-76.
**Kessler, J. O.** (1986). The external dynamics of swimming micro-organisms. *Prog. Phycol. Res.* **4**, 257-291.
**Khalitov, D. A. and Longmire, E. K.** (2002). Simultaneous two-phase PIV by two-parameter phase discrimination. *Exp. Fluids* **32**, 252-268.
**Kiger, K. T. and Pan, C.** (2000). PIV technique for the simultaneous measurement of dilute two-phase flows. *J. Fluids Eng.* **122**, 811-818.
**Kiørboe, T. and Visser, A. W.** (1999). Predator and prey perception in copepods due to hydromechanical signals. *Mar. Ecol. Prog. Ser.* **179**, 81-95.
**Kiørboe, T., Saiz, E. and Visser, A.** (1999). Hydrodynamic signal perception in the copepod *Acartia tonsa*. *Mar. Ecol. Prog. Ser.* **179**, 97-111.
**Koehl, M. A. R. and Hadfield, M. G.** (2010). Hydrodynamics of larval settlement from a larva's point of view. *Integr. Comp. Biol.* **50**, 539-551.
**Koehl, M. A. R. and Reidenbach, M. A.** (2007). Swimming by microscopic organisms in ambient water flow. *Exp. Fluids* **43**, 755-768.
**Komar, P. D. and Reimers, C. E.** (1978). Grain shape effects on settling rates. *J. Geol.* **86**, 193-209.
**Lacalli, T. C. and Gilmour, T. H. J.** (1990). Ciliary reversal and locomotory control in the pluteus larva of *Lytechinus pictus*. *Philos. Trans. R. Soc. Lond. B Biol. Sci.* **330**, 391-396.
**Lebour, M. V.** (1931). The larval stages of *Nassarius reticulatus* and *Nassarius incrassatus*. *J. Mar. Biol. Assoc. UK* **17**, 797-817.
**Mackie, G. O., Singla, C. L. and Thiriot-Quievreux, C.** (1976). Nervous control of ciliary activity in gastropod larvae. *Biol. Bull.* **151**, 182-199.
**Manríquez, P. H. and Castilla, J. C.** (2011). Behavioural traits of competent *Concholepas concholepas* (loco) larvae. *Mar. Ecol. Prog. Ser.* **430**, 207-221.
**Maxey, M. R.** (1987). The gravitational settling of aerosol particles in homogeneous turbulence and random flow fields. *J. Fluid Mech.* **174**, 441-465.
**Maxey, M. R. and Riley, J. J.** (1983). Equation of motion for a small rigid sphere in a nonuniform flow. *Phys. Fluids* **26**, 883-889.
**McDonald, K. A.** (2012). Earliest ciliary swimming effects vertical transport of planktonic embryos in turbulence and shear flow. *J. Exp. Biol.* **215**, 141-151.
**Mei, R., Adrian, R. J. and Hanratty, T. J.** (1991). Particle dispersion in isotropic turbulence under Stokes drag and Basset force with gravitational settling. *J. Fluid Mech.* **225**, 481-495.
**Mohideen, S. K., Perumal, S. A. and Sathik, M. M.** (2008). Image de-noising using discrete wavelet transform. *Int. J. Comput. Sci. Net. Sec.* **8**, 213-216.
**Murakami, A. and Takahashi, K.** (1975). Correlation of electrical and mechanical responses in nervous control of cilia. *Nature* **257**, 48-49.
**Reeks, M. W.** (1977). On the dispersion of small particles suspended in an isotropic turbulent fluid. *J. Fluid Mech.* **83**, 529-546.
**Rubey, W. W.** (1933). Settling velocity of gravel, sand, and silt particles. *Am. J. Sci.* **25**, 325-338.
**Ruiz, J., Macías, D. and Peters, F.** (2004). Turbulence increases the average settling velocity of phytoplankton cells. *Proc. Natl. Acad. Sci. USA* **101**, 17720-17724.
**Saarenrinne, P. and Piirto, M.** (2000). Turbulent kinetic energy dissipation rate estimation from PIV velocity vector fields. *Exp. Fluids* **29**, S300-S307.
**Salazar, J. P. L. C., De Jong, J., Cao, L., Woodward, S. H., Meng, H. and Collins, L. R.** (2008). Experimental and numerical investigation of inertial particle clustering in isotropic turbulence. *J. Fluid Mech.* **600**, 245-256.
**Schwalb, A. N. and Ackerman, J. D.** (2011). Settling velocities of juvenile Lampsilini mussels (Mollusca: Unionidae): the influence of behavior. *J. North Am. Benthol. Soc.* **30**, 702-709.
**Shy, S. S., Tang, C. Y. and Fann, S. Y.** (1997). A nearly isotropic turbulence generated by a pair of vibrating grids. *Exp. Therm. Fluid Sci.* **14**, 251-262.
**Sleigh, M. A. and Blake, J. R.** (1977). Methods of ciliary propulsion and their size limitations. In *Scale Effects in Animal Locomotion* (ed. T. J. Pedley), pp. 243-256. London: Academic Press.
**Srdic, A., Fernando, H. J. S. and Montenegro, L.** (1996). Generation of nearly isotropic turbulence using two oscillating grids. *Exp. Fluids* **20**, 395-397.
**Sutherland, K. R., Dabiri, J. O. and Koehl, M. A. R.** (2011). Simultaneous field measurements of ostracod swimming behavior and background flow. *Limnol. Oceanogr. Fluids Environ.* **1**, 135-146.
**Tanaka, T. and Eaton, J. K.** (2007). A correction method for measuring turbulence kinetic energy dissipation rate by PIV. *Exp. Fluids* **42**, 893-902.
**Taylor, G. I.** (1935). Statistical theory of turbulence. *Proc. R. Soc. Lond. A Math. Phys. Sci.* **151**, 421-444.
**Torrence, C. and Compo, G. P.** (1998). A practical guide to wavelet analysis. *Bull. Am. Meteorol. Soc.* **79**, 61-78.
**Turner, E. J., Zimmer-Faust, R. K., Palmer, M. A., Luckenbach, M. and Pentcheff, N. D.** (1994). Settlement of oyster (*Crassostrea virginica*) larvae: effects of water flow and a water-soluble chemical cue. *Limnol. Oceanogr.* **39**, 1579-1593.
**Vogel, S.** (1994). *Life in Moving Fluids*. Princeton, NJ: Princeton University Press.
**Walker, J. A.** (2002). Functional morphology and virtual models: physical constraints on the design of oscillating wings, fins, legs, and feet at intermediate reynolds numbers. *Integr. Comp. Biol.* **42**, 232-242.
**Wang, L.-P. and Maxey, M. R.** (1993). Settling velocity and concentration distribution of heavy particles in homogeneous isotropic turbulence. *J. Fluid Mech.* **256**, 27-68.
**Weng, W. G., Fan, W. C., Liao, G. X. and Qin, J.** (2001). Wavelet-based image denoising in (digital) particle image velocimetry. *Signal Process.* **81**, 1503-1512.
**Wernet, M. P. and Pline, A.** (1993). Particle displacement tracking technique and Cramer-Rao lower bound error in centroid estimates from CCD imagery. *Exp. Fluids* **15**, 295-307.
**Whitman, E. R. and Reidenbach, M. A.** (2012). Effect of benthic flow environments on recruitment of *Crassostrea virginica* larvae to an intertidal oyster reef habitat. *Mar. Ecol. Prog. Ser.* **463**, 177-191.
**Young, C. M.** (1995). Behavior and locomotion during the dispersal phase of larval life. In *Ecology of Marine Invertebrate Larvae* (ed. L. McEdward), pp. 249-278. Boca Raton, FL: CRC Press.